High pressure effects on the structure and spectroscopy of V^{3+} substitutional defects in Cs_2NaYCl_6. An *ab initio* embedded cluster study

Luis Seijo[a] and Zoila Barandiarán
Departamento de Química, C-XIV and Instituto Universitario de Ciencia de Materiales Nicolás Cabrera, Universidad Autónoma de Madrid, 28049 Madrid, Spain

(Received 22 May 2002; accepted 30 October 2002)

In this paper we present the results of *ab initio* model potential embedded cluster average coupled pair functional calculations on $(VCl_6)^{3-}$ embedded in a reliable representation of the Cs_2NaYCl_6 host. They are aimed at complementing recent high pressure, room temperature, broad band luminescence studies with detailed theoretical data. In particular, we study the effects of high hidrostatic pressure (i) on the structure of V^{3+} substitutional defects in four low lying electronic states (a^3T_{1g}, $^3T_{2g}$, $^1T_{2g}$, and b^3T_{1g}), (ii) on the individual a_{1g} and e_g force constants and equilibrium displacements, and (iii) on the zero-phonon and Franck–Condon energy differences between them. It is shown that only the e_g equilibrum displacements between different electronic sates are large and pressure dependent, while the a_{1g} ones are small and essentially pressure independent. A value of $\kappa=4\times10^{-3}$ kbar^{-1} is suggested for the isothermal bulk modulus of the Cs_2NaYCl_6 elpasolite, because it allows for an excellent match between the theoretical dependence on the unit cell volume and the experimental dependence on applied pressure of several properties: equilibrium displacements, vibrational frequencies, and minimum-to-minimun and vertical energy differences. © *2003 American Institute of Physics.* [DOI: 10.1063/1.1531659]

I. INTRODUCTION

High pressure has long ago been recognized as a very valuable tool for the study of the spectroscopic properties of materials,[1] because it can be used to change the relative energies of the involved states. The availability of diamond and sapphire anvil cells has produced a recent, rising interest in this topic and the number of experimental spectroscopic studies under high pressure is increasing.[2] Very often, these are broad band spectroscopic studies rather than high resolution ones and, as a consequence, the structural information deduced from the analysis of the absorption–emission spectra is limited. In these circumstances, *ab initio* calculations can be used to provide detailed structural information that complements the experiments, so enhancing the usefulness of broad band spectroscopic studies under high pressure.

Recently, Wenger and Güdel[3] carried out a broad band luminescence study of V^{3+}-doped Cs_2NaYCl_6 under high pressure, which was focused on the a^3T_{1g} ground state and the $^3T_{2g}$ and $^1T_{2g}$ excited states of the V^{3+} $3d^2$ configuration, and was aimed at establishing how the pressure affects not only the energy separation between these states, but also the force constants and equilibrium displacements, the latter being an important issue scarcely addressed in similar studies. The a^3T_{1g}, $^3T_{2g}$ and $^1T_{2g}$ states are displaced relative to each other along the a_{1g} and e_g vibrational normal modes[3,4] and, although displacements along other modes are possible, they are not expected to be significant.[5] Since the force constants and the displacements of the different states along a_{1g} and e_g normal coordinates could not be extracted from their broad band and structureless room temperature emission spectra, Wenger and Güdel used the single configurational coordinate model in order to obtain as much information as possible;[3] in this model, an effective nuclear coordinate Q_{eff} is adopted which is some unknown superposition of a_{1g} and e_g normal modes. They found the effective offset between $^3T_{2g}$ and a^3T_{1g} $|\Delta Q_{\text{eff}}|$, to reduce from 0.22 Å at 1 bar to 0.18 Å at 26 kbar, and the effective vibrational frequency of these states, $\bar{\nu}_{\text{eff}}$, to increase from 259 cm^{-1} at 1 bar to 285 cm^{-1} at 26 kbar.

In this paper, we present the results of *ab initio* calculations on the $(VCl_6)^{3-}$ cluster, embedded in a reliable representation of the Cs_2NaYCl_6 lattice. We used the *ab initio* model potential (AIMP) embedded cluster method,[6,7] which was previously proven to be useful in $K_2NaGaF_6:Cr^{3+}$ under high pressure.[8] The results of the calculations on the a_{1g} and e_g energy surfaces of the a^3T_{1g}, $^3T_{2g}$, $^1T_{2g}$, and b^3T_{1g} states of $(VCl_6)^{3-}$ as a function of the Cs_2NaYCl_6 unit cell volume, support the conclusions of Wenger and Güdel;[3] also, these results complement their data with detailed a_{1g} and e_g equilibrium coordinates and vibrational frequencies for these states under high pressure. In particular, we find that the changes with pressure of $\bar{\nu}_{a_{1g}}$ and $\bar{\nu}_{e_g}$ are very similar, whereas the changes of the nuclear displacement offsets $\Delta Q_{a_{1g}}$ and ΔQ_{e_g} are very different: $\Delta Q_{a_{1g}}$ is almost unchanged and ΔQ_{e_g} changes much with pressure. Also, the $T\otimes e$ Jahn–Teller coupling is found to be reduced under high pressure; both the size of the coupling and the size of its pressure dependence are found to be very state dependent. Finally, the comparison of experimental pressure derivatives of transition energies with their corresponding theoretical volume derivatives suggests that the isothermal bulk modulus of Cs_2NaYCl_6 is $\kappa=4\times10^{-3}$ kbar^{-1}; this value is con-

[a]Electronic mail: luis.seijo@uam.es

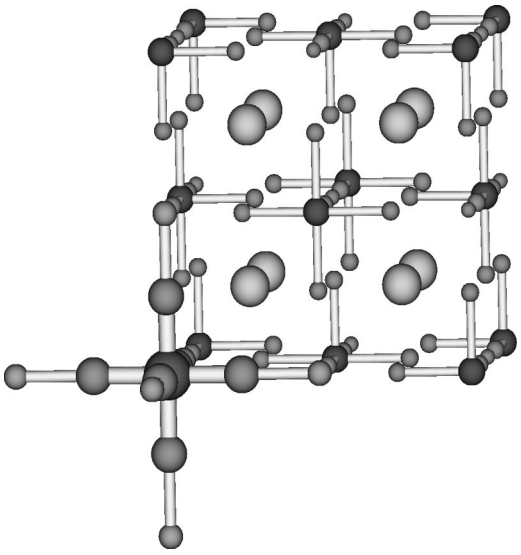

FIG. 1. Unit cell of Cs_2NaYCl_6 with a substitutional V^{3+} defect. The first coordination shell of six Cl^- ions with O_h symmetry has been enhanced, as well as the Na^+ nearest-neighbors (100, 010, 001 directions). Other nearest neighbors to the $(VCl_6)^{3-}$ cluster are Cs^+ions (111 directions).

sistent with the pressure derivatives and volume derivatives of the nuclear displacements offsets and of the vibrational frequencies.

II. METHOD AND DETAILS OF THE CALCULATIONS

The electronic states of V^{3+}-doped Cs_2NaYCl_6 that are the object of interest in this paper are localized in the V^{3+} impurities, which substitute for some of the Y^{3+}ions in an O_h site, and in its first coordination shell of six Cl^- (see Fig. 1.) They correspond to the $3d^2$ open-shell configuration of V^{3+} and, in particular, to the t_{2g}^2 and $t_{2g}^1e_g^1$ configurations of $(VCl_6)^{3-}$, t_{2g} and e_g being the antibonding molecular orbitals of main character of V^{3+}-$3d$. They are the a^3T_{1g} ground state and $^1T_{2g}$ excited state, of main character t_{2g}^2 with some contribution from $t_{2g}^1e_g^1$, and the $^3T_{2g}$ excited state, of the $t_{2g}^1e_g^1$ configuration; we also extended the calculations to the b^3T_{1g} excited state, of main character $t_{2g}^1e_g^1$ with some contribution from t_{2g}^2.

The electronic transitions between these states are mainly influenced by all the atomic interactions within V^{3+} and its bonding interactions with the first coordination shell of Cl^- and, in a smaller although significant amount, by the embedding effects brought about by the rest of the Cs_2NaYCl_6 host. Accordingly, we performed wave function-based *ab initio* embedded cluster calculations. We made complete-active-space self-consistent-field (CASSCF)[9] calculations (with 2 electrons in the t_{2g} and e_g active orbitals,) in a $(VCl_6)^{3-}$ cluster embedded in an *ab initio* model potential (AIMP)[6,7] representation of the Cs_2NaYCl_6 crystalline lattice, in order to produce reliable molecular orbitals. Then, we used the molecular orbitals in average coupled-pair functional (ACPF)[10] calculations that included the correlation effects of 14 electrons in the molecular orbitals of main character V^{3+}-$3d$ (t_{2g}, e_g) and Cl^--$3p$ (t_{2g}, e_g, a_{1g}).[11] This recipe was proposed as a means to reach a reasonable balance between precision and economy in first-series transition metal complexes[11] where the correlation of the 36 $3p$ electrons of the six chlorine ligands are hard to include in multireference ACPF calculations. Furthermore, it was shown to lead to good results in a number of calculations on systems and properties which are similar to the ones under consideration in this work.[7] We used the same Gaussian basis set as that described in Ref. 12, where it was succesfully applied to spectroscopic studies of V^{3+} impurities in several hosts. It is made of a $(14s,11p,6d,3f)/[8s,7p,4d,1f]$ all-electron basis set for V resulting from the Wachters set[13] augmented with d-type diffuse[14] and f-type polarization[15] functions, a $(7s,7p,1d)/[2s,3p,1d]$ valence basis set for Cl[16–18] combined with a [Ne]-core AIMP,[16] and a $(7s,4p)/[1s,1p]$ basis set[19] located at the Na^+ (100, 010, 001) sites which are next-neighbor to the $(VCl_6)^{3-}$ cluster, which is used in order to provide the cluster wave function with the ability to be (quasi) orthogonal to the host wave functions.[20]

In order to study the high pressure effects, we added to the otherwise isolated $(VCl_6)^{3-}$ cluster the AIMP embedding potentials of the Cs_2NaYCl_6 host at several values of the unit cell volume. The embedding potential at ambient pressure was produced in *self-consistent embedded ions* calculations in Ref. 19, where it is fully described. In brief, the embedding potential is made of a sum of 482 total-ion AIMPs of the Cs^+, Na^+, Y^{3+}, and Cl^- ions surrounding the cluster, (each of them made of an electrostatic point-charge plus charge-density local Coulomb potential, a nonlocal exchange potential, and a projection operator that prevents the cluster wave function from collapsing onto the host lattice,) plus 2696 extra point charges which allow for a correct description of the long-range Madelung potential; all of the total-ion AIMPs and point-charges are located at experimental sites $[Cs_2NaYCl_6(O_h^5-F_{m3m})$, $a=10.7396$ Å, $x_{Cl}=0.243\,93]$.[21] The embedding potentials for higher pressures have been produced in this work with the same procedure applied to compressed Cs_2NaYCl_6 lattices of $a=10.6752$, 10.5463, 10.4067, and 10.3530 Å, which correspond to $-\Delta V/V=0.0179$, 0.0530, 0.0902, and 0.1042.[22]

For the Cs_2NaYCl_6 lattice under the five different compressions, we calculated the energy surfaces of the above mentioned states of $(VCl_6)^{3-}$ along the a_{1g} and e_g vibratonal normal modes,[5] from which we extracted the sought energetic and structural information. The a_{1g} breathing mode and the θ component of the degenerate Jahn–Teller active e_g mode are respectively defined as

$$Q_{a_{1g}}=(Z_1-Z_4+X_2-X_5+Y_3-Y_6)/\sqrt{6} \tag{1}$$

and

$$Q_{e_g\theta}=(2Z_3-2Z_6-X_1+X_4-Y_2+Y_5)/\sqrt{12}, \tag{2}$$

where, as an example, Z_1 stands for the displacement of the Cl ligand number 1 with respect to its octahedral equilibrium position along the z Cartesian axis $[Z_1=z(Cl_1)-z_{\mathrm{equil},O_h}(Cl_1)]$, and so on; the Cl ligands 1, 2, and 3 are located on the positive sides of the z, x, and y axes, respectively, and the Cl ligands 4–6 are located on the correspond-

ing negative sides. The basic features of the $T\otimes e$ Jahn–Teller surfaces (Jahn–Teller distortions and stabilization energies) are defined by the cross section of the energy surface along the $Q_{e_g\theta}$ mode alone, so that exploring the other e_g mode, $Q_{e_g\epsilon}$, is unneccessary.[5] The harmonic vibrational frequencies are[5]

$$\omega_{a_{1g}}=\sqrt{\frac{1}{m_{\mathrm{Cl}}}\left(\frac{\partial^2 E}{\partial Q_{a_{1g}}^2}\right)},\quad \omega_{e_g}=\sqrt{\frac{1}{m_{\mathrm{Cl}}}\left(\frac{\partial^2 E}{\partial Q_{e_g\theta}^2}\right)}, \tag{3}$$

where E is the total energy of the embedded cluster and m_{Cl} is the mass of one individual Cl nucleus; the corresponding wave numbers are

$$\overline{\nu}_{a_{1g}}=\omega_{a_{1g}}\times 219\,475\ \mathrm{cm}^{-1},$$
$$\overline{\nu}_{e_g}=\omega_{e_g}\times 219\,475\ \mathrm{cm}^{-1}, \tag{4}$$

if atomic units are used for energies, distances, and masses in Eq. (3). In order to calculate the equilibrium bond distances and the second derivatives in Eq. (3), we calculated the total energies at several values of the V–Cl distances, with step size 0.05 bohr (0.026 Å), and we fitted the values to a third-degree polinomial; after exploring different step sizes and polinomial degrees, the procedure leads to distances and vibrational frequencies that are stable in 0.001 Å and 1 cm^{-1}, respectively. We have not studied here the effects of high pressure on normal modes other than a_{1g} and e_g. The a^3T_{1g}, $^3T_{2g}$, and $^1T_{2g}$ states may show in principle displacements along other normal modes, but they are not expected to be significant[5] and, as a matter of fact, nothing in the experiments indicates that they could be relevant in the present case.[3,4] Furthermore, the displacements along other vibrational modes would not affect our results on the a_{1g} breathing mode and the e_g Jahn–Teller active mode.

Quantum mechanics–molecular mechanics calculations performed in doped elpasolites at ambient pressure[12,19] with the AIMP/shell-model method,[23] have shown that the effects of lattice relaxation beyond the first coordination shell of the impurity ion on bond distances, vibrational frequencies, and spectroscopic transitions are negligible in these materials, as a consequence of the ML_6 clusters being isolated from each other in the material, rather thank linked together. The reductions in the volume of the unit cell brought about by the high pressures under consideration in the present study are relatively small and the previous conclusion is expected to hold here. Accordingly, we have not considered these additional relaxation effects in the present calculations.

All the calculations have been performed with the MOLCAS-5 package.[24]

III. RESULTS AND DISCUSSION

We summarize the calculated structural and spectroscopic data of $(VCl_6)^{3-}$ embedded in Cs_2NaYCl_6 at different pressures in Table I. In addition to the lattice constant, a, and the corresponding unit volume reductions, $-\Delta V/V$, we include the pressure values to which they correspond if the isothermal bulk modulus is $\kappa=4\times10^{-3}$ kbar^{-1}; we will later justify the assumption of this value. Note that all the calculated variations with pressure in this Section assume this value of the bulk modulus. The following data are shown in the Table: R_e is the V–Cl equilibrium distance in the a_{1g} breathing mode of $(VCl_6)^{3-}$ and $\overline{\nu}_{a_{1g}}$ is the corresponding vibrational frequency. $\Delta Q_{a_{1g}}$ is the offset of the a_{1g} massless nuclear coordinate with respect to the ground state a^3T_{1g}, $\Delta Q_{a_{1g}}=\sqrt{6}\,\Delta R_e$. $\delta_{e_g\theta}$ is the nuclear displacement coordinate along the $e_g\theta$ vibrational mode: $R(\mathrm{V–Cl}_X)=R(\mathrm{V–Cl}_Y)=R_e-\delta_{e_g\theta}$, $R(\mathrm{V\text{-}Cl}_Z)=R_e+2\,\delta_{e_g\theta}$, and $\Delta Q_{e_g\theta}$ is the offset of the $e_g\theta$ massless nuclear coordinate with respect to the ground state, $\Delta Q_{e_g\theta}=\sqrt{12}\,\Delta\delta_{e_g\theta}$.

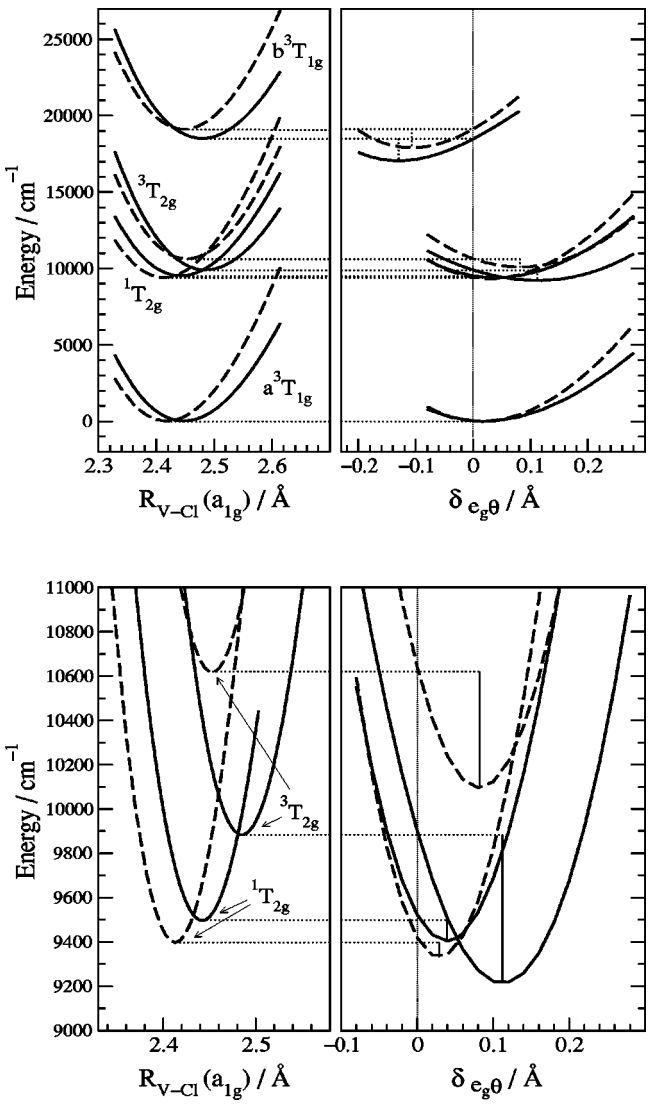

FIG. 2. Energy surfaces of the a^3T_{1g}, $^3T_{2g}$, $^1T_{2g}$, and b^3T_{1g} states of $(VCl_6)^{3-}$ embedded in Cs_2NaYCl_6 along the a_{1g} and $e_g\theta$ vibrational coordinates. Full lines: $\Delta V/V=0$. Dashed lines: $\Delta V/V=-0.1042$, which corresponds to a pressure of 26 kbar assuming $\kappa=4\times10^{-3}$ kbar^{-1}. See text for a description. The $^3T_{2g}$ and $^1T_{2g}$ energy surfaces are enhanced in the bottom part of the figure.

TABLE I. Effects of high pressure on the potential energy surfaces of low lying states of Cs_2NaYCl_6: $(VCl_6)^{3-}$. See text for a description. Distances in Å, vibrational frequencies and energies in cm^{-1}.

	lattice constant, a	10.7396	10.6752	10.5463	10.4067	10.3530
	$-\Delta V/V$	0	0.0179	0.0530	0.0902	0.1042
	pressure [a]	1 bar	4.5 kbar	13.2 kbar	22.5 kbar	26 kbar
R_e	a^3T_{1g}	2.448	2.444	2.434	2.422	2.418
	$^3T_{2g}$	2.485	2.480	2.470	2.458	2.453
	$^1T_{2g}$	2.442	2.438	2.429	2.417	2.413
	b^3T_{1g}	2.479	2.475	2.464	2.452	2.448
$\Delta Q_{a_{1g}}$	$^3T_{2g}$	0.091	0.089	0.088	0.088	0.086
	$^1T_{2g}$	−0.014	−0.014	−0.013	−0.013	−0.012
	b^3T_{1g}	0.076	0.075	0.073	0.073	0.073
$\overline{\nu}_{a_{1g}}$	a^3T_{1g}	294	297	306	314	318
	$^3T_{2g}$	295	299	306	316	320
	$^1T_{2g}$	293	296	305	314	317
	b^3T_{1g}	295	299	306	316	320
$\delta_{e_g\theta}$	a^3T_{1g}	0.018	0.017	0.016	0.015	0.014
	$^3T_{2g}$	0.112	0.107	0.096	0.086	0.082
	$^1T_{2g}$	0.039	0.038	0.033	0.031	0.029
	b^3T_{1g}	−0.130	−0.126	−0.119	−0.110	−0.107
$\Delta Q_{e_g\theta}$	$^3T_{2g}$	0.326	0.312	0.277	0.246	0.236
	$^1T_{2g}$	0.071	0.070	0.060	0.055	0.052
	b^3T_{1g}	−0.513	−0.495	−0.468	−0.433	−0.419
$\overline{\nu}_{e_g}$	a^3T_{1g}	210	214	224	236	240
	$^3T_{2g}$	181	186	197	209	214
	$^1T_{2g}$	209	213	223	235	238
	b^3T_{1g}	241	244	250	257	260
E_{JT} $(T\otimes e)$	a^3T_{1g}	26	25	23	21	21
	$^3T_{2g}$	699	670	615	562	544
	$^1T_{2g}$	114	113	100	91	87
	b^3T_{1g}	1471	1431	1347	1259	1224
minimum to minimum transitions						
T_e (a_{1g})	$^3T_{2g}$	9884	9987	10 222	10 500	10 619
	$^1T_{2g}$	9498	9487	9455	9414	9398
	b^3T_{1g}	18 486	18 573	18 771	19 004	19 105
$T_e(a_{1g}+e_g)$	$^3T_{2g}$	9214	9346	9626	9959	10 096
	$^1T_{2g}$	9408	9399	9373	9345	9331
	b^3T_{1g}	17 044	17 170	17 443	17 767	17 901
ΔE_e [b]	(a_{1g})	386	500	767	1086	1221
	$(a_{1g}+e_g)$	−194	−53	253	614	765
vertical (Franck–Condon) transitions						
$a^3T_{1g}\rightarrow{}^3T_{2g}$ [d]	(a_{1g})	10 287	10 390	10 625	10 904	11 029
	$(a_{1g}+e_g)$	10 090	10 200	10 441	10 730	10 863
$\rightarrow{}^1T_{2g}$ [d]	(a_{1g})	9505	9495	9463	9422	9406
	$(a_{1g}+e_g)$	9446	9438	9406	9375	9362
$\rightarrow b^3T_{1g}$ [d]	(a_{1g})	18 774	18 860	19 059	19 294	19 399
	$(a_{1g}+e_g)$	19 220	19 282	19 458	19 675	19 756
$^3T_{2g}\rightarrow a^3T_{1g}$ [e]	(a_{1g})	−9516	−9619	−9844	−10 121	−10 246
	$(a_{1g}+e_g)$	−8354	−8500	−8821	−9188	−9347
$\rightarrow b^3T_{1g}$ [f]	(a_{1g})	8610	8594	8559	8514	8494
	$(a_{1g}+e_g)$	12 388	12 225	11 857	11 517	11 379
$b^3T_{1g}\rightarrow a^3T_{1g}$ [e]	(a_{1g})	−18 222	−18 301	−18 503	−18 728	−18 835
	$(a_{1g}+e_g)$	−15 094	−15 255	−15 586	−16 000	−16 163
$^1T_{2g}\rightarrow{}^3T_{2g}$	(a_{1g})	1003	1028	1299	1622	1752
	$(a_{1g}+e_g)$	599	719	1023	1352	1494

[a] Assuming a bulk modulus $\kappa=4\times10^{-3}$ $kbar^{-1}$.
[b] $\Delta E_e=T_e(^3T_{2g})-T_e(^1T_{2g})$. To be compared with ΔE_o of Wenger and Güdel (Ref. 3); see Fig. 3(a).
[c] To be compared with $-E_{center}$ of Wenger and Güdel (Ref. 3); see Fig. 3(b).
[d] Absorption.
[e] Emission.
[f] Excited state absorption, ESA.

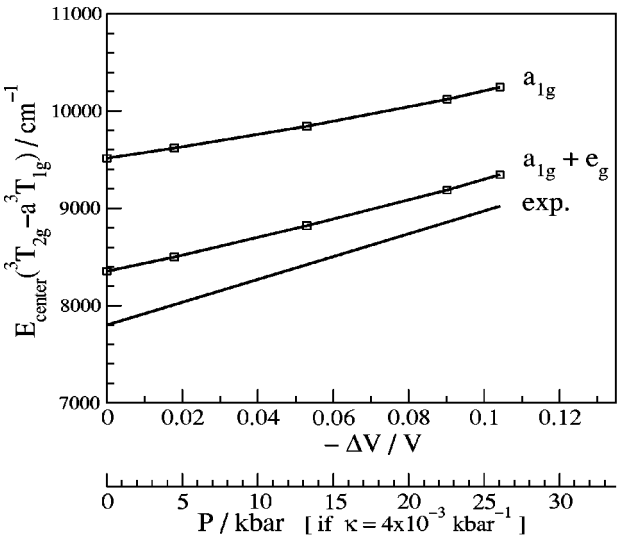

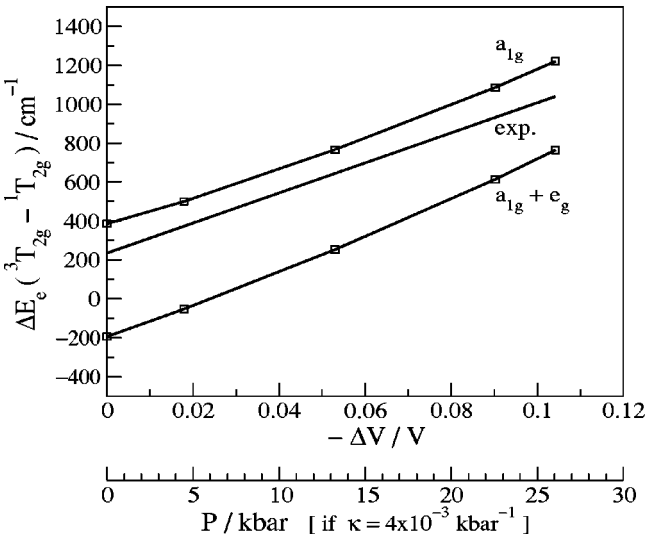

FIG. 3. (a) Franck–Condon $^3T_{2g} \rightarrow a^3T_{1g}$ emission as calculated in the a_{1g} and $a_{1g}+e_g$ energy surfaces, and experimental emission baricenter (linear regression fit to the 1 bar–18 kbar, from Ref. 3) as a function of pressure. (b) Calculated minimum-to-minimum energy difference between the excited states $^3T_{2g}$ and $^1T_{2g}$ in the a_{1g} and $a_{1g}+e_g$ energy surfaces, and zero-phonon energy difference as deduced from experimental luminescence decay rate constants (Ref. 3) as a function of pressure.

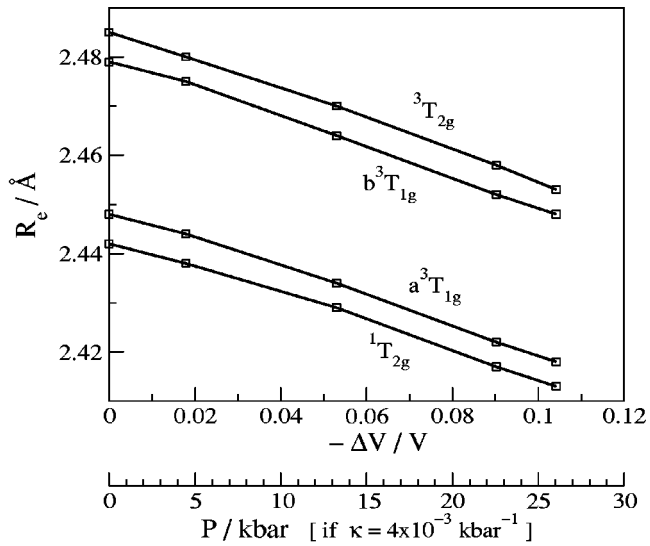

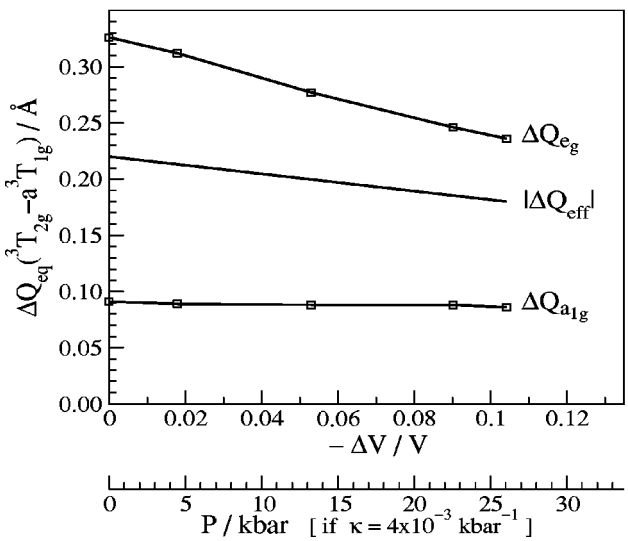

FIG. 4. (a) a_{1g} breathing mode V–Cl equilibrium distance of $(VCl_6)^{3-}$ embedded in Cs_2NaYCl_6 as a function of lattice compression. (b) Calculated offsets of the a_{1g} and e_g massless nuclear coordinates of the $^3T_{2g}$ excited state with respect to the ground state a^3T_{1g}, as a function of lattice compression. The absolute value of the effective mode experimental offset (Ref. 3, estimated at 1 bar and 26 kbar, and connected with a straight line) is also shown for comparison.

E_{JT} $(T \otimes e)$ stands for the Jahn–Teller stabilizaton energy of the $T \otimes e$ vibronic coupling problem. T_e stands for minimum to minimum energy differences with the a^3T_{1g} ground state; the rest of energy differences are vertical ones (Franck–Condon) calculated at the minimum of the initial state. Energy differences in the a_{1g} breathing mode are tabulated together with those in the $a_{1g}+e_g$ vibrational modes. The energy surfaces at ambient pressure and at $\Delta V/V = -0.1042$ are shown in Fig. 2 and the effects of compression on the most relevant structural and spectroscopic data of Table I are shown in Figs. 3–6.

Recently, Wenger and Güdel[3] have measured the pressure dependence of some structural and spectroscopic parameters of V^{3+}-doped Cs_2NaYCl_6. From the direct observation of the $^3T_{2g} \rightarrow a^3T_{1g}$ room temperature wide luminescence (full width at half maximum of around 2000 cm^{-1}) they find the band baricenter to change from 7800 cm^{-1}at 1 bar to 9022 cm^{-1}at 26 kbar, with $dE_{\text{center}}/dp = 47$ cm^{-1}/kbar. We present their measurements in Fig. 3(a) together with our calculations of the Franck–Condon emission energy, calculated as the energy difference between the $^3T_{2g}$ and a^3T_{1g} states at the equilibrium structure of $^3T_{2g}$. The lattice compression increases this transition energy, as corresponds to the fact that it is essentially proportional to the crystal field splitting,[25] which increases with the bond shortening produced by the compression. As it can be observed, consideration of the e_g distortions suffered by the T states as a consequence of the $T \otimes e$ Jahn–Teller vibronic coupling[5] is not neccesary in order to describe the pressure dependence of the emission band baricenter; however, the e_g distortions are responsible for lowering the value of this emission by 1000 cm^{-1}, approximately. We find a lattice compression depen-

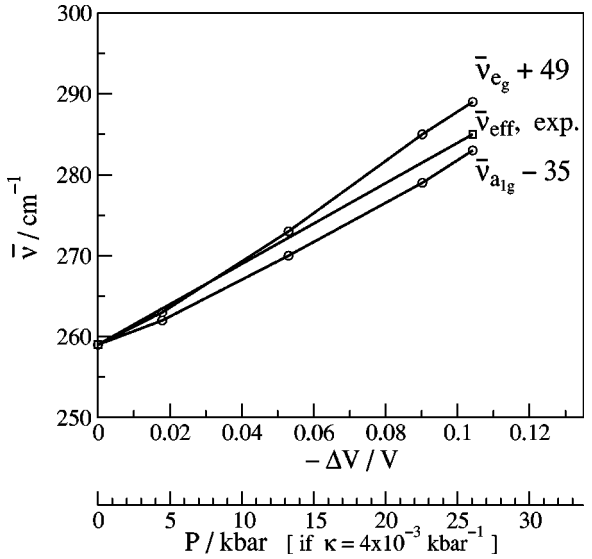

FIG. 5. Calculated a_{1g} and e_g vibrational frequencies of the a^3T_{1g} ground state and experimental effective mode vibrational frequency (Ref. 3, estimated at 1 bar and 26 kbar, and connected with a straight line) as a function of lattice compression.

dence of the emission band maximum of $dE_{\text{center}}/d(-\Delta V/V) = 9530\ \text{cm}^{-1}$.

In addition, Wenger and Güdel find $d\Delta E_o/dp = 31\ \text{cm}^{-1}/\text{kbar}$, ΔE_o being the energy difference between the zero-phonon levels of the $^3T_{2g}$ and $^1T_{2g}$ excited states, from the fitting of a reasonable equation for the room temperature luminescence decay rate constant as a function of pressure to the experimental data. We show their result in Fig. 3(b) together with our calculations of the minimum-to-minimum energy difference between the excited states $^3T_{2g}$ and $^1T_{2g}$, ΔE_e, in the a_{1g} and $a_{1g}+e_g$ energy surfaces. We observe, again, that the e_g distortions are not neccesary for a correct

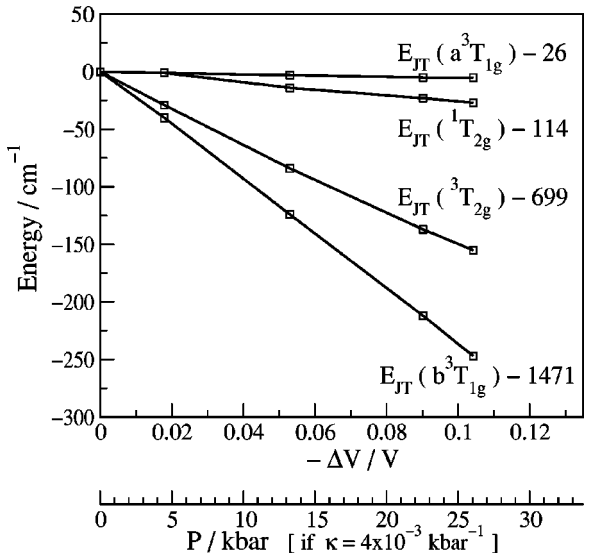

FIG. 6. Calculated $T\otimes e$ Jahn–Teller stabilization energies of the a^3T_{1g}, $^3T_{2g}$, $^1T_{2g}$, and b^3T_{1g} states as a function of lattice compression. All of them have been shifted as indicated in order to emphasize their different pressure dependence.

description of the changes of this quantity with lattice compression. After considering them, a disagreement of 400 cm^{-1} exists between experiments and the present calculations in the absolute value of this quantity; this result is good and it is in the limit of what can be expected from state of the art *ab initio* calculations in these systems. We find a lattice compression dependence of the energy mimimum separation between $^3T_{2g}$ and $^1T_{2g}$ of $d\Delta E_e/d(-\Delta V/V) = 9203\ \text{cm}^{-1}$. This dependence and the one of the $^3T_{2g}\rightarrow a^3T_{1g}$ emission band maximum shown above fit well with the experimental measurements of their respective pressure dependence if the isothermal bulk modulus of the Cs_2NaYCl_6 material is $\kappa = 4\times10^{-3}\ \text{kbar}^{-1}$. We will assume this value from now on. Similar values of κ have been obtained in shell-model simulations of this material.[26]

Let us now comment on the defect structures and on their pressure dependence. In Fig. 4(a), we can see the a_{1g} bond distances and their dependence with the lattice compression. The values of the bond distance of the four states at any pressure agree with the expected picture: The t_{2g}^2 configuration leads to shorter bond distance than the $t_{2g}^1e_g^1$ configuration, as a consequence of the crystal field stabilization of the t_{2g} antibonding molecular orbitals relative to the e_g antibonding molecular orbitals;[25] the $t_{2g}-e_g$ crystal field splitting is proportional to $1/R_{\text{V-Cl}}^5$ in crystal field theory, so that the $t_{2g}\rightarrow e_g$ excitation energy adds to the total energy of the states of the t_{2g}^2 configuration a contribution that decreases with the V–Cl distance and that, in consequence, results in a larger bond distance for the $t_{2g}^1e_g^1$ configuration.[25] As a result, the order of bond distances agrees with that of $t_{2g}^1e_g^1$ character: $^1T_{2g} < \approx a^3T_{1g} < b^3T_{1g} < \approx {}^3T_{2g}$. It is clear in Fig. 4(a) that the four states show an almost identical bond distance dependence on the unit cell volume and on the pressure, [all of them have $dR_e/d(-\Delta V/V) = -0.29$ Å and $dR_e/dp = -0.0012$ Å/kbar], which leads to an almost negligible effect of pressure on the a_{1g} offsets $\Delta Q_{a_{1g}}$ [see the $^3T_{2g}-a^3T_{1g}$ a_{1g} offset in Fig. 4(b)]. On the contrary, the e_g distortions suffered by the four T states as a consequence of the $T\otimes e$ Jahn–Teller vibronic coupling, are very different (see $\delta_{e_g\theta}$ in Table I) and they show different quantitative effects of pressure (the absolute value of the e_g distortion is always reduced by pressure). As a result, the e_g offsets, ΔQ_{e_g}, are very sensitive to the lattice compression, in opposition to the a_{1g} offsets. This is illustrated in Fig. 4(b), where we show the calculated a_{1g} and e_g offsets between the $^3T_{2g}$ and a^3T_{1g} states, together with the experimental value of the effective mode offset as deduced from the analysis of the $^3T_{2g}\rightarrow a^3T_{1g}$ luminescence[3] (note that only the absolute value of the offset can be deduced from that analysis of the emission spectrum). It is clear from Fig. 4(b) that the present *ab initio* calculation support the interpretation of Wenger and Güdel[3] since the effective mode offset, which is supposed to be a mixture of the a_{1g} and e_g ones, shows a pressure dependence intermediate to both of them. Moreover, the *ab initio* calculations allow to complete this interpretation by stating that the changes in the effective mode offset produced by pressure are essentially due to the pressure effects on the offset of the e_g Jahn–Teller active mode.

Lattice compression rises force constants at the time that reduces bond distances. The effective mode vibrational frequency deduced from the analysis of the ${}^3T_{2g} \rightarrow a^3T_{1g}$ emission, which is assumed to be equal for both states, increases from 259 cm^{-1} at 1 bar to 285 cm^{-1} at 26 kbar, with $d\bar{\nu}_{\text{eff}}/dp = 1$ cm^{-1}/kbar.[3] Our calculations show that the four states under study have very similar a_{1g} vibrational frequencies, which in addition show an almost equal pressure dependence. They have, however, different e_g vibrational frequencies: ${}^1T_{2g}$ and a^3T_{1g}, of almost identical t_{2g}^2 configurational character, show very similar $\bar{\nu}_{e_g}$, whereas ${}^3T_{2g}$ has a smaller one, the three of them having very similar pressure dependence; b^3T_{1g}, however, has a much larger $\bar{\nu}_{e_g}$ with a softer increase with lattice compresion. In Fig. 5 we present the experimental $\bar{\nu}_{\text{eff}}$ together with the calculated $\bar{\nu}_{a_{1g}}$ and $\bar{\nu}_{e_g}$ of the ground-state a^3T_{1g}, which have been shifted for a better comparison of the pressure dependence of the three vibrational frequencies. It is again clear that the present calculations support the interpretation of Ref. 3 at the time that are able to provide a few more details: The effective mode vibrational frequency pressure dependence results from a slightly smoother dependence of the a_{1g} frequency and a slightly steeper dependence of the e_g frequency.

We may remark here that the agreement between the experimental pressure dependence of $\bar{\nu}_{\text{eff}}$ and the calculated $\Delta V/V$ dependence of $\bar{\nu}_{a_{1g}}$ and $\bar{\nu}_{e_g}$ shown in Fig. 5, as well as between the experimental pressure dependence of ΔQ_{eff} and the calculated $\Delta V/V$ dependence of $\Delta Q_{a_{1g}}$ and ΔQ_{e_g} in Fig. 4(b), further support the value of $\kappa = 4 \times 10^{-3}$ $kbar^{-1}$ previously assumed for Cs_2NaYCl_6 after the analysis of the ${}^3T_{2g} \rightarrow a^3T_{1g}$ emission band maximum and of the energy mimimum separation between ${}^3T_{2g}$ and ${}^1T_{2g}$.

Finally, we show in Fig. 6 the $T \otimes e$ Jahn–Teller (JT) stabilization energies of the four states under study; they are shifted for a better sight of their different lattice compression dependence. They all are linear with pressure with negative slope in the interval under study, $E_{\text{JT}}(a^3T_{1g})$ is very small and insensitive to lattice compression, $E_{\text{JT}}({}^1T_{2g})$ is small and shows a very smooth variation with pressure, $E_{\text{JT}}({}^3T_{2g})$ is large and suffers a significant reduction with pressure ($dE_{\text{JT}}/dp = -6$ cm^{-1}/kbar), and $E_{\text{JT}}(b^3T_{1g})$ is very large and with a big pressure dependence ($dE_{\text{JT}}/dp = -9.5$ cm^{-1}/kbar). The reduction with pressure of the Jahn–Teller stabilization energies of the four states is consistent with the reduction of the distortions along the e_g Jahn–Teller active mode (see above) and it reflects that pressure lowers the the size of the Jahn–Teller coupling in all the states under study.

IV. CONCLUSIONS

The present *ab initio* ACPF calculations on the $(VCl_6)^{3-}$ cluster embedded in a Cs_2NaYCl_6 crystalline lattice support the interpretation of recent high pressure, room temperature, broad band luminescence experiments on V^{3+}-doped Cs_2NaYCl_6,[3] and the structural data that have been deduced from them by means of the use of a single effective configurational coordinate model, which is assumed to be a mixture of a_{1g} and e_g modes. Moreover, the calculations complement all that information with detailed quantitative data on the individual a_{1g} and e_g vibrational modes which was not possible to extract from the experiments: In particular, we present the analysis of the effects of high pressure (i) on the individual equilibrium nuclear coordinates and their offsets, which shows that only the e_g offses are pressure dependent, (ii) on the individual vibrational frequencies, which shows that both of them exhibit a very similar pressure dependence, (iii) on the $T \otimes e$ Jahn–Teller vibronic coupling stabilization energy, which shows that their absolute values and their variation with pressure are very state specific, the size of the JT coupling being always lowered by pressure, and (iv) on the a_{1g} and e_g contributions to the minimum-to-minimum and Franck–Condon transition energies between the states a^3T_{1g}, ${}^3T_{2g}$, ${}^1T_{2g}$, and b^3T_{1g}. Finally, a value of $\kappa = 4 \times 10^{-3}$ $kbar^{-1}$ is suggested for the isothermal bulk modulus of Cs_2NaYCl_6: If we assume it, we find a very good match between the *ab initio* embedded cluster calculations of the dependence of nuclear coordinates, force constants, and state energy differences on the unit cell volume, on the one side, and their experimental dependence with pressure, on the other.

In summary, it is shown that wave function based *ab initio* embedded cluster calculations provide complementary information that enhances the usefulness of high pressure, room temperature, broad band spectroscopic studies.

ACKNOWLEDGMENT

This work was partly supported by a grant from Ministerio de Ciencia y Tecnología, Spain (Dirección General de Investigación, PB98-0108).

[1] H. G. Drickamer, in *Solid State Physics*, edited by F. Seitz and D. Trunbull (Academic, New York, 1965), Vol. 17, p. 1.
[2] K. L. Bray, *Topics in Current Chemistry* (Springer, Berlin, 2001), Vol. 213.
[3] O. S. Wenger and H. Güdel, Chem. Phys. Lett. **354**, 75 (2002).
[4] C. Reber and H. U. Güder, J. Lumin. **42**, 1 (1988).
[5] I. B. Bersuker, *The Jahn–Teller Effect and Vibronic Interactions in Modern Chemistry* (Plenum, New York and London, 1984).
[6] Z. Barandiarán and L. Seijo, J. Chem. Phys. **89**, 5739 (1988).
[7] L. Seijo and Z. Barandiarán, in *Computational Chemistry: Reviews of Current Trends*, edited by J. Leszczynski (World Scientific, Singapore, 1999), Vol. 4, p. 55.
[8] L. Seijo, Z. Barandiarán, and L. G. M. Pettersson, J. Chem. Phys. **98**, 4041 (1993).
[9] B. O. Roos, P. R. Taylor, and P. E. M. Siegbahn, Chem. Phys. **48**, 157 (1980); P. E. M. Siegbahn, A. Heiberg, J. Almlöf, and B. O. Roos, J. Chem. Phys. **74**, 2384 (1981); P. Siegbahn, A. Heiberg, B. Roos, and B. Levy, Phys. Scr. **21**, 323 (1980).
[10] R. Ahlrichs, P. Scharf, and C. Ehrhardt, J. Chem. Phys. **82**, 890 (1985); R. J. Gdanitz and R. Ahlrichs, Chem. Phys. Lett. **143**, 413 (1988).
[11] K. Pierloot and L. G. Vanquickenborne, J. Chem. Phys. **93**, 4154 (1990).
[12] A. Al-Abdalla, L. Seijo, and Z. Barandiarán, J. Mol. Struct.: THEOCHEM **451**, 135 (1998).
[13] A. J. H. Wachters, J. Chem. Phys. **52**, 1033 (1970).
[14] P. J. Hay, J. Chem. Phys. **66**, 4377 (1977).
[15] L. G. M. Pettersson (private communication).
[16] S. Huzinaga, L. Seijo, Z. Barandiarán, and M. Klobukowski, J. Chem. Phys. **86**, 2132 (1987).
[17] T. H. Dunning and P. J. Hay, in *Modern Theoretical Chemistry*, edited by H. F. Schaefer III (Plenum, New York, 1977).

[18] J. Andzelm, M. Klobukowski, E. Radzio-Andzelm, Y. Sakai, and H. Tatewaki, *Gaussian Basis Sets for Molecular Calculations*, edited by S. Huzinaga (Elsevier, Amsterdam, 1984).
[19] A. Al-Abdalla, Z. Barandiarán, L. Seijo, and R. Lindh, J. Chem. Phys. **108**, 2005 (1998).
[20] J. L. Pascual, L. Seijo, and Z. Barandiarán, J. Chem. Phys. **98**, 9715 (1993).
[21] C. Reber, H. U. Güdel, G. Meyer, T. Schleid, and C. A. Daul, Inorg. Chem. **28**, 3249 (1989).
[22] The data of these and other core/embedding AIMPs are available from the authors upon request or directly at the address http://www.uam.es/quimica/aimp/Data/AIMPLibs.html
[23] J. L. Pascual and L. Seijo, J. Chem. Phys. **102**, 5368 (1995).
[24] MOLCAS Version 5, K. Andersson, M. Barysz, A. Bernhardsson *et al.*, Lund University, Sweden, 2000.
[25] S. Sugano, Y. Tanabe, and H. Kamimura, *Multiplets of Transition-Metal Ions in Crystal* (Academic, New York, 1970).
[26] A. M. Woods *et al.*, J. Phys. Chem. Solids **54**, 543 (1993).